Journal Name

ARTICLE TYPE

Cite this: DOI: 00.0000/xxxxxxxxxx

Decoding the Chemical Bond—On the Connection between Probability Density Analysis, QTAIM, and VB Theory†

Leonard Reuter[a] and Arne Lüchow*[a]

Received Date
Accepted Date

DOI: 00.0000/xxxxxxxxxx

Classification of bonds is essential for understanding and predicting the reactivity of chemical compounds. This classification mainly manifests in the bond order and the contribution of different Lewis resonance structures. Here, we outline a first principles approach to obtain these orders and contributions for arbitrary wave functions in a manner that is both, related to the quantum theory of atoms in molecules and consistent with valence bond theory insight: the Lewis structures arise naturally as attractors of the all-electron probability density $|\Psi|^2$. Doing so, we introduce a valence bond weight definition that does not collapse in the basis set limit.

1 Introduction

While modern computers allow for the ever more accurate computation of molecular properties with advanced quantum mechanical methods, chemists continue to think in Lewis structures and qualitative valence bond concepts like hybridization. This qualitative view of molecular chemistry, which is often called 'chemists intuition', has proven to be an essential tool in predicting and explaining reactions and is thus unlikely to vanish or substantially change in the near future.

In order to connect these two worlds of chemistry, the qualitative concepts have to be redefined and rediscovered in the mathematical framework of quantum mechanics. Reaching this goal would allow chemists to adapt their intuition to theoretical insight that goes beyond energies, geometries, and dipole moments.

While a lot has already been achieved—mainly in the context of valence bond (VB) theory and the quantum theory of atoms in molecules (QTAIM)—there is no method that is both, universally applicable to any wave function and capable of capturing the many-particle nature of electronic systems.

In the present work, we will try to take a small step towards the desired redefinition and universal applicability by investigating the topology of the all-electron probability density $|\Psi|^2$ and by providing maps to qualitative concepts of bond classification. We call this approach 'probability density analysis' (PDA). In order to gain a comprehensive picture of chemical bonding, the PDA results are compared with the established VB theory and QTAIM.

A century ago—and ten years before Schrödinger's equation[1]—Lewis laid the foundations of molecular bond classification.[2,3] Heitler and London subsequently developed valence bond theory by merging Lewis concept of 'electron pairs' into wave mechanics.[4] Eventually, Pauling generalized the theory by writing molecular wave functions as linear combinations of Lewis resonance structures.[5] Later work improved the computability[6] and accuracy[7] of VB theory.

Meanwhile, Bader and Beddall introduced what would later become the quantum theory of atoms in molecules, a 'unified theory of atoms, bonds, structure, and structural stability' which is based on partitioning the 3D real space into topological quantum atoms defined by the electronic density.[8–10] Chamorro et al.[11] and later Martín Pendás and coworkers[12–17] integrated the probability density $|\Psi|^2$ over the quantum atoms in order to gain insight into the all-electron distribution. QTAIM and VB Theory have already been compared by Zhang et al.[18], Ferro-Costas and Mosquera[19], and Martín Pendás and Francisco.[20]

More recently, Scemama et al.[21] picked up the idea of investigating the maxima of $|\Psi|^2$, which was pioneered by Artmann[22] and by Zimmermann and Rysselberghe.[23] However, they discarded the approach in favor of the maximum probability domains. Lüchow and coworkers reintroduced the topological analysis of $|\Psi|^2$,[24] added the definition of a basin as the 3N-dimensional analogue to the quantum atom,[25] and used this partitioning to investigate the anomeric effect.[26] This topological analysis of $|\Psi|^2$ is now relabelled as probability density analysis (PDA). It should be noted that Schmidt and coworkers recently and successfully followed a similar approach.[27–30] On the experimental side, Waitz et al. showed that the many-electron probability density $|\Psi|^2$ is—in principle—measurable.[31]

In order to obtain a comprehensive picture of chemical bonding in molecules, the three aforementioned approaches (i.e. VB

[a] Institute of Physical Chemistry, RWTH Aachen University, Landoltweg 2, 52074 Aachen, Germany. Tel: +49 241 80 94748; E-mail: luechow@rwth-aachen.de

† Electronic Supplementary Information (ESI) available: energies and weights for all investigated systems. See DOI: 00.0000/00000000.

theory, QTAIM, and PDA) should be combined and compared. In the present work, this comparison is done in detail for the simplest system H_2. While QTAIM and VB theory have already been compared for this system by Ferro-Costas and Mosquera,[19] we think that their conclusion might be misleading and follow the approach by Martín Pendás and Francisco instead.[20] A range of single bonds (heteroatomic and homoatomic) are calculated in order to confirm and generalize the H_2 results. Finally, the different approaches are compared for double bonds in ethylene, ozone, and sulfur dioxide.

2 Methods

In this section, the term 'attractor' is used synonymous with 'local maximum'. It is borrowed from dynamical system theory and is linked with the term 'basin of attraction'.

All investigated wave functions $\Psi(\mathbf{R})$ are linear combinations of configuration state functions (CSFs) $\Phi_K(\mathbf{R})$. The CSFs themselves are linear combinations of Slater determinants $\psi_k(\mathbf{R})$.

$$\Psi(\mathbf{R}) = \sum_K C_K \Phi_K(\mathbf{R}) = \sum_K C_K \sum_k c_{Kk} \psi_k(\mathbf{R}) \tag{1}$$

In a self-consistent iterative optimization, the so-called configuration interaction coefficients C_K are optimized simultaneously with the orbitals, while the linear coefficients c_{Kk} are fixed.

For the complete active space self-consistent field (CASSCF) method, the determinants are built from an orthonormal set of molecular orbitals and the c_{Kk} are called 'spin coupling coefficients'. The resulting CASSCF CSFs form an orthonormal basis themselves.

The valence bond self-consistent field (VBSCF) method by van Lenthe and Balint-Kurti[6] is an alternative to CASSCF. It is one of the modern valence bond methods which use wave functions that are built from inactive molecular orbitals and active strictly localized hybrid atomic orbitals.

In VB terminology, the CSFs are called (VB) structures. In addition to their mathematical representation, each structure can be depicted in the graphical Lewis representation, see Fig. 1.

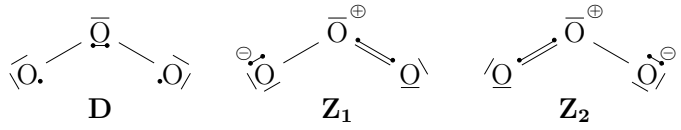

Fig. 1 Example of the Lewis representation—three structures of the π system in ozone with formal charges. Labels are taken from Braïda et al.[32]

The importance of structures is quantified with weights W_k which are (almost) always positive and sum up to one. In the three most common definitions, the weights depend on the structure overlap matrix $\mathbf{S}$:

$$S_{IJ} = \int_{\mathbb{R}^{3N}} \mathrm{d}\mathbf{R}\, \Phi_I(\mathbf{R}) \Phi_J(\mathbf{R}) \tag{2}$$

The Chirgwin-Coulson weight

$$W_K^{\mathrm{CC}} = C_K \sum_L C_L S_{KL} \tag{3}$$

is the most intuitive definition and follows directly from partitioning the norm of the probability density:

$$\int_{\mathbb{R}^{3N}} \mathrm{d}\mathbf{R}\, |\Psi_{\mathrm{VB}}(\mathbf{R})|^2 = \sum_K C_K \sum_L C_L S_{KL} \tag{4}$$

It is closely related to the Mulliken population analysis: multiplication of the structure weights with the respective formal charges (e.g. see Fig. 1) produces the Mulliken partial charges. The Löwdin weight[33]

$$W_K^{\mathrm{Löw.}} = \left(\sum_L C_L S_{KL}^{1/2} \right)^2 \tag{5}$$

is an alternative which is analogous to the Löwdin population analysis. The inverse weight

$$W_K^{\mathrm{inv.}} = \frac{\alpha_K}{\sum_L \alpha_L}, \qquad \alpha_K = \frac{C_K^2}{S_{KK}^{-1}} \tag{6}$$

by G. A. Gallup and J. M. Norbeck[34] is often discussed as another alternative. It should be noted that for orthonormal CSFs ($S_{IJ} = \delta_{IJ}$) like those employed in CASSCF all definitions give $W_K = C_K^2$. The problem of VB weight definition thus arises solely from the non-orthogonality of the CSFs .

In quantum theory of atoms in molecules, attractors of the electronic density $\rho(\mathbf{r})$ are denoted nuclear critical points. They partition the real space $\mathbb{R}^3$ into their basins of attraction $\boldsymbol{\omega}$ which are commonly referred to as Bader basins. Their surfaces $s(\boldsymbol{\omega})$ are of zero flux in the gradient vector field of $\rho(\mathbf{r})$:

$$\nabla\rho(\mathbf{r}) \cdot \mathbf{n}(\mathbf{r}) = 0, \qquad \forall \mathbf{r} \in s(\boldsymbol{\omega}) \tag{7}$$

with the position vector $\mathbf{r} \in \mathbb{R}^3$ and the unit vector $\mathbf{n}(\mathbf{r})$ normal to the surface $s(\boldsymbol{\omega})$.

The formalism of electron number distribution functions (EDFs) by Martín Pendás and coworkers[12–17]—and pioneered by Chamorro et al.[11]—gives additional insight into the statistical distribution of electrons. Most commonly, the Bader basins presented above are used for integration, however any set of basins that partition $\mathbb{R}^3$ could be used.

For EDF, every point $\mathbf{R}$ in the $3N$-dimensional all-electron space is mapped to a partition $\mathscr{S} = (n_1, n_2, \ldots, n_m)$ by the partition assignment function σ which assigns every electron individually to the basin $\boldsymbol{\omega}_I$ it is found in, then counts the number of electrons n_I per basin $\boldsymbol{\omega}_I$ for $I = 1, \ldots, m$.

A $3N$-domain $\mathscr{D}_i$ can be defined for every partition $\mathscr{S}_i$:

$$\mathscr{D}_i = \{\mathbf{R} \in \mathbb{R}^{3N} | \sigma(\mathbf{R}) = \mathscr{S}_i\} \tag{8}$$

The probability $p(\mathscr{S}_i)$ of a partition can be calculated by integrating the all-electron probability density $P(\mathbf{R}) = |\Psi(\mathbf{R})|^2 / \int_{\mathbb{R}^{3N}} \mathrm{d}\mathbf{R} |\Psi(\mathbf{R})|^2$ over the domain $\mathscr{D}_i$:

$$p(\mathscr{S}_i) = \int_{\mathscr{D}_i} \mathrm{d}\mathbf{R}\, P(\mathbf{R}) \tag{9}$$

If it is possible to map a partition to a VB resonance structure (ie. $\mathscr{S}_i \to \Phi_K$), an EDF weight can be defined: $W_K^{\mathrm{EDF}} = p(\mathscr{S}_i)$

However, with the Bader basins alone, this map does often not

exist (eg. for multiple bonds). Instead, a partition can then be mapped to a group of resonance structures, that have the same formal charges.

In probability density analysis[24–26]—pioneered by Scemama et al.[21]—, attractors of the probability density $P(\mathbf{R})$ partition the all-electron position space $\mathbb{R}^{3N}$ into their basins of attraction $\boldsymbol{\Omega}$. The surfaces $S(\boldsymbol{\Omega})$ of these basins are of zero flux in the gradient vector field of $P(\mathbf{R})$:

$$\nabla P(\mathbf{R}) \cdot \mathbf{N}(\mathbf{R}) = 0, \qquad \forall \mathbf{R} \in S(\boldsymbol{\Omega}) \tag{10}$$

with the all-electron position vector $\mathbf{R} \in \mathbb{R}^{3N}$ and the unit vector $\mathbf{N}(\mathbf{R})$ normal to the surface $S(\boldsymbol{\Omega})$. For one-electron systems (e.g. H_2^+) PDA is identical to QTAIM, since $\mathbf{R} = \mathbf{r}$ and thus $P(\mathbf{R}) \equiv \rho(\mathbf{r})$. The attractors of $P(\mathbf{R})$ can be assigned to VB structures (more precisely VB determinants) and the integral of $P(\mathbf{R})$ over a basin of attraction can be interpreted as a measure of importance. We therefore define the PDA weight of a VB structure

$$W_K^{\mathrm{PDA}} = \int_{\boldsymbol{\Omega}_K} \mathrm{d}\mathbf{R}\, P(\mathbf{R}) \tag{11}$$

where Ω_K is the union of all basins Ω around attractors that are assigned to determinants of the VB structure Φ_K.

In general, a good agreement of VB theory and PDA is expected due to the locality of VB orbitals: if a Slater determinant is built from perfectly localized orbitals (in the sense of no overlap of the squared orbitals), the squared Slater determinant is the sum of squares of all possible Hartree products. The attractors of the squared determinant are then composed of the 3D attractors of the squared orbitals—this has already been pointed out by Scemama et al.[21] While the VB orbitals cannot be perfectly localized (otherwise there would be no bonding), a good agreement of the all-electron attractors with the squared orbitals attractors is still expected.

3 Computational Approach

The VB program XMVB[35,36] has been used for all VB calculations. The integrals have been prepared with Gaussian 16.[37] The Molpro[38] package has been used for all CASSCF calculations. Experimental geometries are taken from NIST Computational Chemistry Comparison and Benchmark Database[39] for the following molecules: HF and HCl from the NIST Diatomic Spectral Database.[40] H_2O_2 from Redington et al.[41] O_3, SO_2, C_2H_6, and NH_3 from Herzberg.[42] N_2H_4 from Tsuboi and Overend.[43] H_2 and F_2 from Huber and Herzberg.[44] H_2O from Hoy and Bunker.[45] BH_3 from Kuchitsu.[46]

The all-electron triple-ζ Slater type basis set TZPae[47] by van Lenthe and Baerends has been used for the all-electron calculations. For the Gaussian and Molpro calculations the basis functions have each been expanded into 14 primitive Gaussian type functions.[48,49] The energy-consistent pseudopotentials by Burkatzki et al.[50] with the triple-ζ basis set (BFD-VTZ) have been used for ozone and sulfur dioxide. The PDA as well as the stochastic EDF analysis have been performed with our in-house codes Amolqc and inPsights. The PDA integral in Equation 11 is calculated by Monte Carlo integration: samples of the all-electron position vector $\mathbf{R}$ drawn from $P(\mathbf{R})$ are obtained during a variational quantum Monte Carlo run. Local optimization of $P(\mathbf{R})$ (small-step gradient following) is used to identify the attractor of the basin each 3N-dimensional sample point is in.

The EDF integral in Equation 9 is also calculated by Monte Carlo integration, but with local optimization of $\rho(\mathbf{r})$, which is obtained from a B3LYP[51–54] density functional theory calculation (with the VWN(III)[55] local correlation energy) with Molpro.

4 Results and Discussion

4.1 Starting Simple: the Ionic Contribution in H_2

There are several reasons to start with the sandbox molecule H_2: it is easy to understand, two-particle density surface plots on the bond axis can be visualized, the two-particle density is simply the probability density ($\rho_2(\mathbf{r}_1,\mathbf{r}_2) = P(\mathbf{R})$), and it has already been investigated for comparison of QTAIM with VB theory.[19,20]

The hydrogen molecule is oriented along the z-axis, with the mass center at the origin. The protons are labelled A and B and placed at $\mathbf{r}_A\,(0,0,-d_{\mathrm{HH}}/2)$ and $\mathbf{r}_B\,(0,0,d_{\mathrm{HH}}/2)$ respectively. The wave function is built from the two 1s orbitals $\varphi_A(\mathbf{r})$ and $\varphi_B(\mathbf{r})$ with overlap s.

A flexible VB wave function is investigated with all methods:

$$\Psi^{\mathrm{VB}}_{\mathrm{H_2}}(\mathbf{R}) = N^{\mathrm{VB}}_{\mathrm{H_2}} \left[(1-\eta)\, \Psi^{\mathrm{cov.}}_{\mathrm{H_2}}(\mathbf{R}) + \eta\, \Psi^{\mathrm{ion.}}_{\mathrm{H_2}}(\mathbf{R}) \right] \tag{12}$$

$N^{\mathrm{VB}}_{\mathrm{H_2}}$ is the normalization factor, and η controls the contribution of the two normalized VB structures (covalent and ionic)

$$\begin{aligned} \Psi^{\mathrm{cov.}}_{\mathrm{H_2}}(\mathbf{R}) &= \frac{1}{\sqrt{2+2s^2}} \left[\varphi_A(\mathbf{r}_1)\varphi_B(\mathbf{r}_2) + \varphi_B(\mathbf{r}_1)\varphi_A(\mathbf{r}_2) \right] \\ \Psi^{\mathrm{ion.}}_{\mathrm{H_2}}(\mathbf{R}) &= \frac{1}{\sqrt{2+2s^2}} \left[\varphi_A(\mathbf{r}_1)\varphi_A(\mathbf{r}_2) + \varphi_B(\mathbf{r}_1)\varphi_B(\mathbf{r}_2) \right]. \end{aligned} \tag{13}$$

For $\eta = 1/2$, Equation 12 yields the Hartree-Fock (HF) wave function σ_g^2.

4.1.1 QTAIM and EDF

In the electronic density $\rho^{\mathrm{VB}}_{\mathrm{H_2}}(\mathbf{r})$, the ionic coefficient η appears only in the product $\eta\,(1-\eta)$. The density is thus equal for η and $1-\eta$:

$$\begin{aligned} \rho^{\mathrm{VB}}_{\mathrm{H_2}}(\mathbf{r}) &= \frac{\left(N^{\mathrm{VB}}_{\mathrm{H_2}}\right)^2}{s^2+1} \left[(q+1) \left(\varphi_A^2(\mathbf{r}) + \varphi_B^2(\mathbf{r}) \right) - 2\,(q-s)\, \varphi_A(\mathbf{r})\varphi_B(\mathbf{r}) \right] \\ &\text{with} \qquad q = 2\eta\,(1-\eta)\,(s-1) \end{aligned} \tag{14}$$

Therefore, the ionic and covalent VB structures give rise to an identical electronic density which is already mentioned in textbooks.[56] It also follows, that—for the chosen wave function ansatz—the mapping $\rho_{\mathrm{H_2}}(\mathbf{r}) \to \Psi_{\mathrm{H_2}}(\mathbf{R})$ is only unique for the HF wave function ($\eta = 1/2$).

For any η, due to symmetry, the real space $\mathbb{R}^3$ is trivially divided into two Bader basins:

$$\boldsymbol{\omega}_A = \{\mathbf{r} \in \mathbb{R}^3 | r_3 < 0\}, \qquad \boldsymbol{\omega}_B = \{\mathbf{r} \in \mathbb{R}^3 | r_3 > 0\} \tag{15}$$

In order to determine the covalent and ionic contributions of any

approximate wave function, the norm of the probability density (which is also the two-particle density) can be partitioned:

$$
\begin{aligned}
&||P_{H_2}(\mathbf{R})|| = 1 = \int_{\mathbb{R}^3} d\mathbf{r}_1 \int_{\mathbb{R}^3} d\mathbf{r}_2 \, P_{H_2}(\mathbf{R}) \\
&= \left(\int_{\boldsymbol{\omega}_A} d\mathbf{r}_1 \int_{\boldsymbol{\omega}_B} d\mathbf{r}_2 + \int_{\boldsymbol{\omega}_B} d\mathbf{r}_1 \int_{\boldsymbol{\omega}_A} d\mathbf{r}_2 + \int_{\boldsymbol{\omega}_A} d\mathbf{r}_1 \int_{\boldsymbol{\omega}_A} d\mathbf{r}_2 + \int_{\boldsymbol{\omega}_B} d\mathbf{r}_1 \int_{\boldsymbol{\omega}_B} d\mathbf{r}_2 \right) P_{H_2}(\mathbf{R}) \\
&= W_{\text{cov.}}^{\text{EDF}} + W_{\text{ion.}}^{\text{EDF}} \\
&\text{with} \qquad W_{\text{cov.}}^{\text{EDF}} = \left(\int_{\boldsymbol{\omega}_A} d\mathbf{r}_1 \int_{\boldsymbol{\omega}_B} d\mathbf{r}_2 + \int_{\boldsymbol{\omega}_B} d\mathbf{r}_1 \int_{\boldsymbol{\omega}_A} d\mathbf{r}_2 \right) P_{H_2}(\mathbf{R}) \\
&\text{and} \qquad W_{\text{ion.}}^{\text{EDF}} = \left(\int_{\boldsymbol{\omega}_A} d\mathbf{r}_1 \int_{\boldsymbol{\omega}_A} d\mathbf{r}_2 + \int_{\boldsymbol{\omega}_B} d\mathbf{r}_1 \int_{\boldsymbol{\omega}_B} d\mathbf{r}_2 \right) P_{H_2}(\mathbf{R})
\end{aligned}
\tag{16}
$$

Note that this partitioning is but the application of the EDF method by Martín Pendás and coworkers with the covalent partition $\mathscr{S}_{\text{AB}} = (1,1)$ and the ionic partitions $\mathscr{S}_{AA} = (2,0)$ and $\mathscr{S}_{BB} = (0,2)$, which they already used for a comparison with VB Theory.[20] Note also that, in contrast to the work by Ferro-Costas et al.,[19] the whole two-particle density is taken into consideration and not just its exchange-correlation component. The reported conceptual incompatibilities of VB theory and QTAIM are owed to the neglect of $\rho(\mathbf{r}_1)\rho(\mathbf{r}_2)$ which becomes $P_{H_2}(\mathbf{R})$ in the dissociation limit. In accordance with Ferro-Costas et al., we define

$$
I = \int_{\boldsymbol{\omega}_A} d\mathbf{r} \, |\varphi_A(\mathbf{r})|^2 = \int_{\boldsymbol{\omega}_B} d\mathbf{r} \, |\varphi_B(\mathbf{r})|^2 \tag{17}
$$

$W_{\text{ion.}}^{\text{EDF}}$ is a function of η, I, and s with the latter two depending on d_{HH}:

$$
W_{\text{ion.}}^{\text{EDF}} = \frac{(s-1)^2 \eta^2 - \left[s^2 - 2s - 4I(I-1) \right] \eta + \frac{s^2}{2} - 2I(I-1)}{s^2 + 1 - 2\eta(1-\eta)(s-1)^2} \tag{18}
$$

4.1.2 VB Theory

The structure overlap matrix $\mathbf{S}_{H_2}$ is given as

$$
\mathbf{S}_{H_2} = \begin{pmatrix} 1 & S_{\text{ic}} \\ S_{\text{ic}} & 1 \end{pmatrix}, \qquad S_{\text{ic}} = \frac{2s}{s^2+1} \tag{19}
$$

with the ionic-covalent overlap S_{ic}. Its inverse and square root can be calculated as:

$$
\mathbf{S}_{H_2}^{-1} = \begin{pmatrix} S^{-1} & -S_{\text{ic}} S^{-1} \\ -S_{\text{ic}} S^{-1} & S^{-1} \end{pmatrix}, \qquad S^{-1} = \frac{1}{1 - S_{\text{ic}}^2} \tag{20}
$$

$$
\mathbf{S}_{H_2}^{1/2} = \begin{pmatrix} S_+^{1/2} & S_-^{1/2} \\ S_-^{1/2} & S_+^{1/2} \end{pmatrix}, \quad S_\pm^{1/2} = \frac{1}{2} \left(\sqrt{1 + S_{\text{ic}}^2} \pm \sqrt{1 - S_{\text{ic}}^2} \right) \tag{21}
$$

The three VB weights of the ionic structure are calculated according to Eqs. 3-6:

$$
W_{\text{ion.}}^{\text{CC}} = \left(N_{\text{VB}}^{H_2} \right)^2 \left(\eta^2 + \eta(1-\eta) S_{\text{ic}} \right) \tag{22}
$$

$$
W_{\text{ion.}}^{\text{Löw.}} = \left(N_{\text{VB}}^{H_2} \right)^2 \left(\eta S_+^{1/2} + (1-\eta) S_-^{1/2} \right)^2 \tag{23}
$$

$$
W_{\text{ion.}}^{\text{inv.}} = \frac{\eta^2}{\eta^2 + (1-\eta)^2} \tag{24}
$$

Note that $W_{\text{ion.}}^{\text{inv.}}$ is independent of d_{HH}: S^{-1} cancels out because $\mathbf{S}_{H_2}^{-1}$ is persymmetric. It is thus for this system equal to the renormalized weight $W_K^{\text{ren.}} = C_K^2 / \sum_L C_L^2$ which is later in this work omitted due to its independence of the overlap matrix.

4.1.3 PDA

Four attractors $\mathbf{R}_1$-$\mathbf{R}_4$ of $P_{H_2}(\mathbf{R})$ are identified with PDA (see Fig. 2a): $\mathbf{R}_1 = (\mathbf{r}_A, \mathbf{r}_B)$, $\mathbf{R}_2 = (\mathbf{r}_B, \mathbf{r}_A)$, $\mathbf{R}_3 = (\mathbf{r}_A, \mathbf{r}_A)$, and $\mathbf{R}_4 = (\mathbf{r}_B, \mathbf{r}_B)$. The attractors $\mathbf{R}_1$ and $\mathbf{R}_2$ have one electron at each core and can thus be assigned to the covalent structure, while $\mathbf{R}_3$ and $\mathbf{R}_4$ are assigned to the two ionic structures. A covalent and an ionic basin can be defined as unions of the respective basins of attraction $\boldsymbol{\Omega}_1$-$\boldsymbol{\Omega}_4$, which partition $\mathbb{R}^6$.

$$
\boldsymbol{\Omega}_{\text{cov.}} = \boldsymbol{\Omega}_1 \cup \boldsymbol{\Omega}_2, \qquad \boldsymbol{\Omega}_{\text{ion.}} = \boldsymbol{\Omega}_3 \cup \boldsymbol{\Omega}_4 \tag{25}
$$

$W_{\text{ion.}}^{\text{PDA}}$ is obtained by solving the integral of Equation 11 for $\boldsymbol{\Omega}_{\text{ion.}}$ with Monte Carlo integration. Figure 2 shows a comparison of the PDA basins and the QTAIM integration domains defined in Equation 16 which are used for EDF.

4.1.4 Comparison

The presented ionic weight definitions are functions of the ionic coefficient η and of the proton-proton distance d_{HH}, on which s and I depend. The weight-coefficient dependency is shown in Figure 3 for all definitions at three distances.

In the dissociation limit, all definitions agree: they converge to $C_{\text{ion.}}^2$, since $S_{\text{ic}} \to 0$.

In the fused-core limit, $W^{\text{Löw.}}$ and W^{EDF} converge to $1/2$, W^{CC} converges to η, and W^{PDA} seems to converge towards the distance-independent $W^{\text{inv.}}$.

At all distances, all weight definitions agree for the Hartree-Fock wave function ($\eta = 1/2$).

At the equilibrium distance ($d_{\text{HH}} = 1.40 a_0$), W^{PDA} is in between W^{CC} and $W^{\text{inv.}}$, which are the most widely used VB weights. The EDF and Löwdin weights are qualitatively different from the other definitions, since they give a significant ionicity larger than 35% for $\eta = 0$. This qualitative difference should always be kept in mind when discussing VB weights.

A last remark should be added regarding the inverse weights: in contrast to a claim in the original publication, the inverse weight definition does not—in general—'diminish the importance of the ionic terms'. It rather—due to the sigmoidal shape of the curve—diminishes the importance of terms, which already have a low importance.

4.2 Ionic Contributions in Single Bonds

The ionic contribution to any single bond can be calculated similarly to the analysis of H_2 described in the previous section. However, the attractors in $\mathbb{R}^{3N}$ are not as trivial with electron positions away from the nuclei.[24,25] The mapping of attractors $\mathbf{R}_i$ to VB determinants can still be done visually, as shown in Figure 4 for difluorine.

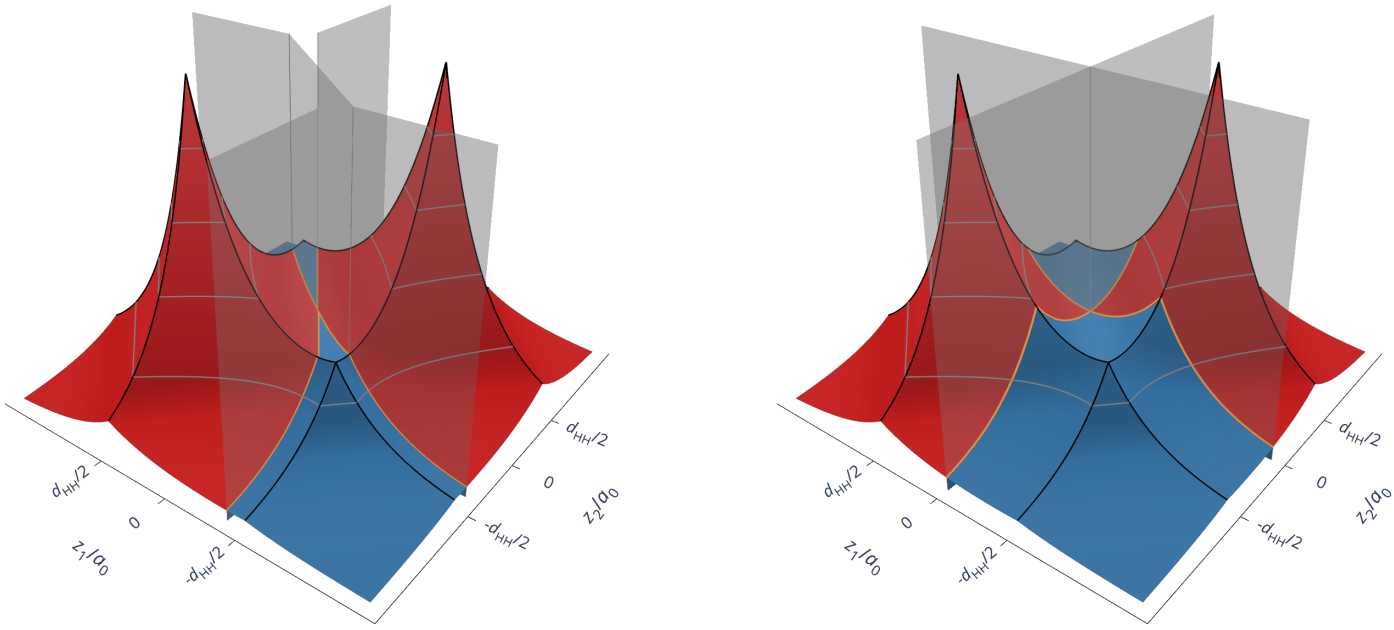

(a) PDA basins $\mathbf{\Omega}$.

(b) QTAIM domains $\mathscr{D}$ used for EDF.

Fig. 2 $P_{H_2}(\mathbf{r}_1,\mathbf{r}_2)$ with $\eta = 0.1$ and $d_{HH} = 1.40\,a_0$ for $\mathbf{r}_1 = (0,0,z_1)$ and $\mathbf{r}_2 = (0,0,z_2)$ (both electrons on the bond axis). The four peaks are the four attractors $\mathbf{R}_1$-$\mathbf{R}_4$. The covalent domain is depicted in red, the ionic domain in blue.

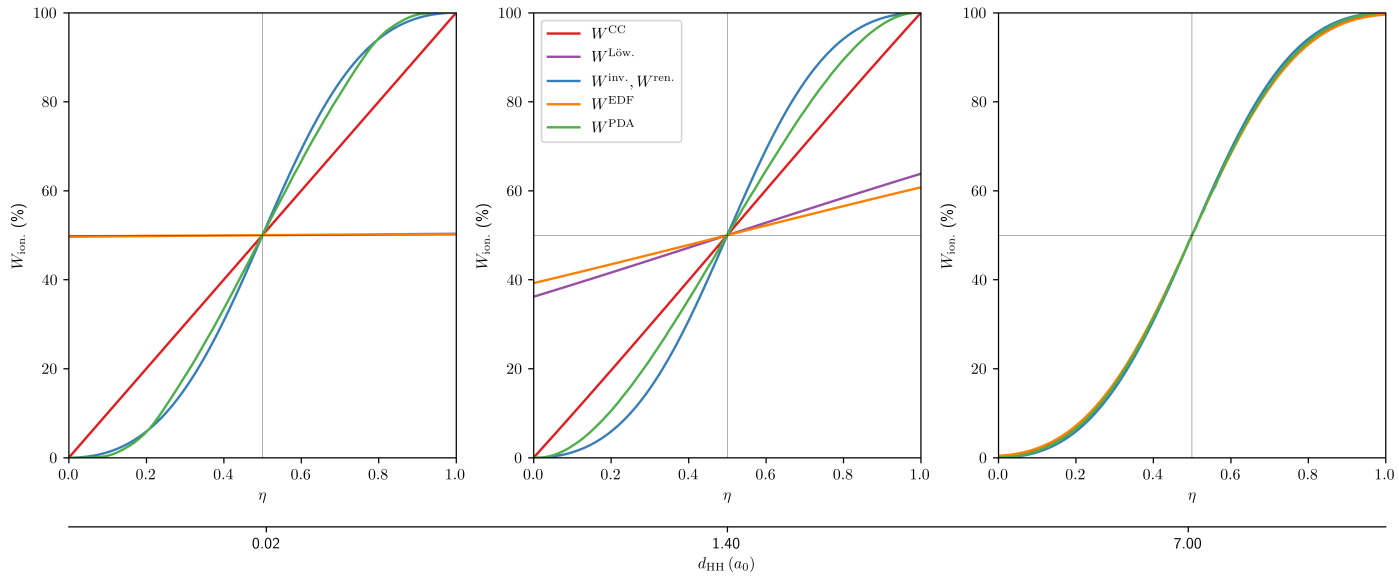

Fig. 3 Different ionic weight definitions as a function of the ionic coefficient η. Comparison for three different proton-proton distances.

(a) covalent (84 %)

(b) ionic 1 (8 %)

(c) ionic 2 (8 %)

Fig. 4 Three attractors of difluorine with VBSCF(2,2). PDA weights in brackets. The fluorine nuclei are depicted as green spheres, electrons as small red or blue spheres depending on their m_s quantum number. Pairs of spin-up and spin-down electrons are connected by purple lines in order to highlight the resemblance to the VB structures.

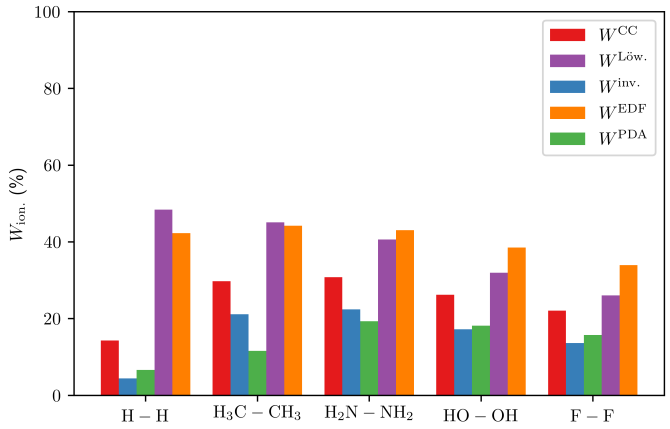

Fig. 5 Ionic contribution according to different definitions for homoatomic bonds.

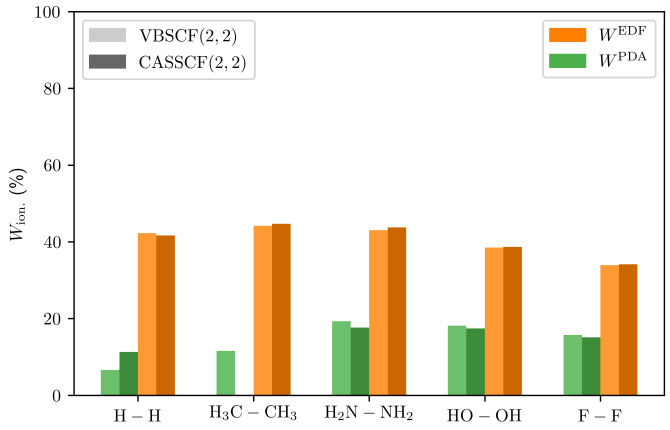

Fig. 6 Ionic contribution from EDF and PDA calculations for CASSCF and VBSCF wave functions.

4.2.1 Homoatomic Bonds

The ionicities for the homoatomic bonds in dihydrogen, ethane, hydrazine, hydrogen peroxide, and difluorine have been calculated using VBSCF(2,2)/TZPae wave functions (see Fig. 5). Again, a good agreement can be observed between the PDA and the inverse weight and between the EDF and the Löwdin weight. The results confirm the qualitative difference between these two pairs of definitions. Since the EDF and PDA weights can be calculated for arbitrary wave functions, the VBSCF(2,2) wave functions are compared with the corresponding CASSCF(2,2) ones in Figure 6. Except for the PDA weight of the C-C bond in ethane, the results of the different wave functions are in good agreement which is expected since both methods are similar and can even be identical in a minimal basis. The larger difference for W^{PDA} in ethane could result from the inactive orbitals being delocalized in CASSCF and block localized in VBSCF.

4.2.2 Heteroatomic Bonds

For hydrogen containing heteroatomic bonds (with VBSCF/TZPae wave functions), the PDA and inverse weights are again found to be in good agreement (see Fig. 7). In contrast to the homoatomic

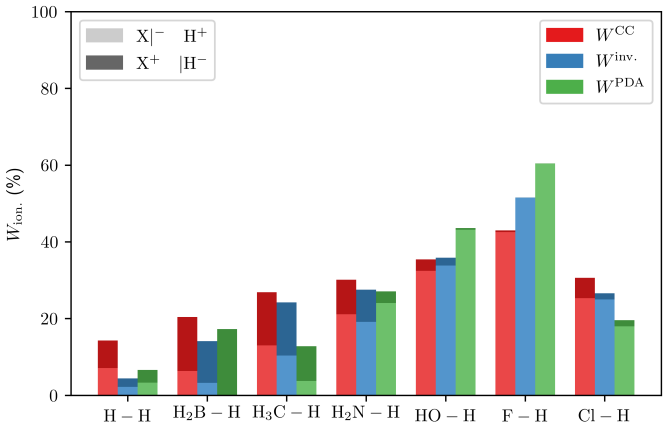

Fig. 7 Ionic contribution according to different definitions for hydrogen containing heteroatomic bonds. The darker coloured parts of the bars are the contributions of the respective hydride ionic structures.

bonds the weights of the two ionic structures are no longer identical due to the lack of symmetry. The PDA and inverse weights are also in good agreement for the resulting individual ionic structures contributions ('X|$^-$ H$^+$' and 'X$^+$ |H$^-$').

4.3 Double Bonds

The characterization of double bonds is only indirectly possible with methods based on the one- or two-electron density like QTAIM and even EDF.

4.3.1 Ethylene

The double bond in ethylene has two different VB representations: the σ-π picture that is widely taught and applied in organic chemistry and the τ-bond where sp^3 hybrids form two 'banana bonds', see Fig. 8. VBSCF(4,4) wave functions built according to the two pictures give rise to almost the same electronic energy. This is expected, since unitary transformation of active orbitals with a subsequent CI optimization does not alter the wave function. There is thus, at first sight, no representation generally favorable. However, if restricted to the most important VB structure, the σ-π wave function is lower in energy by about 13.7 mE_h. If restricted to 3 structures, this difference reduces to 2.4 mE_h (see Fig. 9). For three structures and for the full twenty structures, the energies of the VBSCF(4,4) wave functions are in between the HF energy and the CASSCF(4,4) energy. The energy difference between the CAS and full VB calculations arises largely due to the block localization of the inactive VB orbitals.

The three by inverse weight most important VB structures of the τ VB wave function are depicted in Figure 10. When applying PDA to the VBSCF(4,4) or CASSCF(4,4) wave functions of ethylene, three kinds of attractors are found, see Fig. 11. Note that the two ionic structures are found more frequently in correlated wave functions.[25] These attractors can be rationalized by comparing them to the schematic VB structures of the τ picture in Figure 10. Nearly identical PDA weights are obtained for the both full VB wave functions and the CAS wave function.

The EDF analysis of the investigated wave functions reproduces

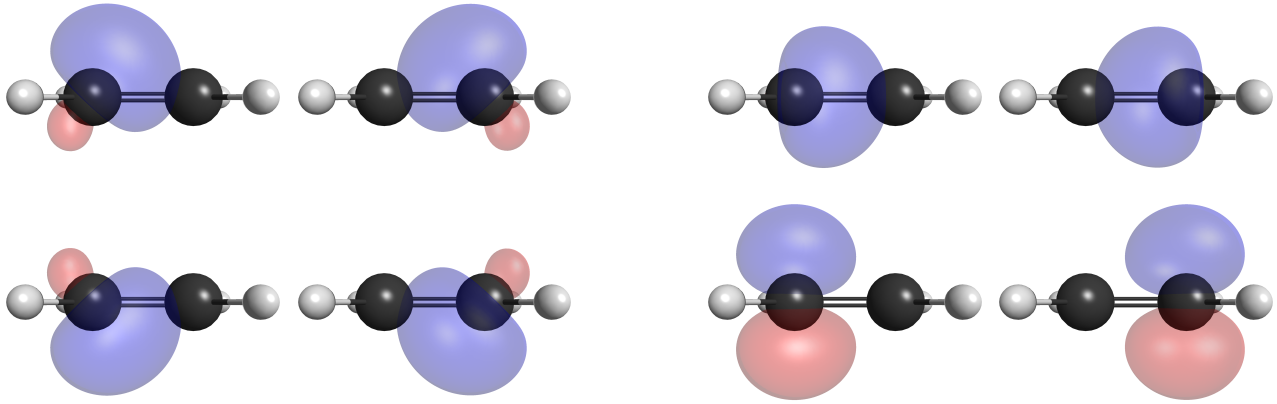

(a) sp^3-hybrids forming τ bonds (Pauling). **(b)** σ-π representation (Hückel).

Fig. 8 Alternative sets of hybrid atomic orbitals for describing the double bond in ethylene with VB theory.

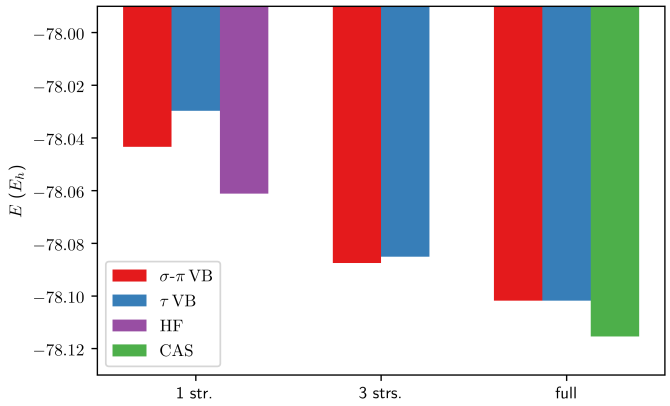

Fig. 9 Electronic energies of different wave functions of ethylene. The optimized active orbitals of the full VB wave functions are shown in Figure 8.

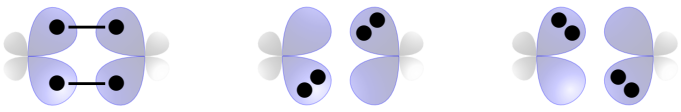

(a) cov. (55%, 84%) **(b)** ionic 1 (9%, 8%) **(c)** ionic 2 (9%, 8%)

Fig. 10 The three most important VB structures of the τ VB wave function with inverse weights for both, the full (20 structure) wave function and the three structure wave function.

the distribution presented by Martín Pendás and Francisco.[17] The EDF analysis with Bader basins cannot distinguish between the three structures in Figure 10 since they have the same formal charges: none. Thus—in order to compare PDA and VB weights with the partition probabilities—the 20 VB structures are grouped according to the distribution of electrons to the CH_2 fragments: in 10 structures, they are distributed evenly (i.e. (8,8)). In 8 structures, both fragments have an absolute formal charge of 1 (i.e. (7,9) and (9,7)) and in 2 structures, the absolute formal charge is 2 (i.e. (6,10) and (10,6)). The sum of the weights of the respective structures can directly be compared to the partition probabilities which are again taken as EDF weights—e.g. $W^{\mathrm{EDF}}_{(8,8)} = p(8,8)$.

Note, that the three structures of Figure 10, which are found as PDA attractors (Fig. 11), are all in the group (8,8). For the defined groups of structures, the PDA weights again agree best with the inverse VB weights (Fig. 12). They are however qualitatively different since only (8,8) structures are found with PDA. The EDF weights are again in good agreement with the Löwdin weights. The EDF and PDA weights of the groups are equal up to 0.5% for the two full VB wave functions and the CAS wave function. Figure 12 thus only shows the results for the full τ VB wave function.

In summary, it can be stated that there are arguments for both double bond pictures in ethylene. While the σ-π picture allows for more compact wave functions, the τ picture is found with PDA for both VB wave functions as well as for the CAS wave function. The most likely arrangement of electrons is thus in agreement with Paulings τ bonds. As discussed in Section 2, this agreement can be explained with the overlap of the squared active orbitals, which is lower in the τ picture.

Furthermore, the close link between VB theory, QTAIM/EDF, and PDA is confirmed for the double bond in ethylene.

(a) covalent (97.1 %) **(b)** ionic 1 (1.4 %) **(c)** ionic 2 (1.4 %)

Fig. 11 Three attractors of ethylene with full VBSCF(4,4). PDA weights in brackets. The carbon nuclei are depicted as dark grey spheres, protons as light grey spheres, electrons as small red or blue spheres depending on their m_s quantum number. Pairs of spin-up and spin-down electrons are connected by purple lines in order to highlight the resemblance to the VB structures.

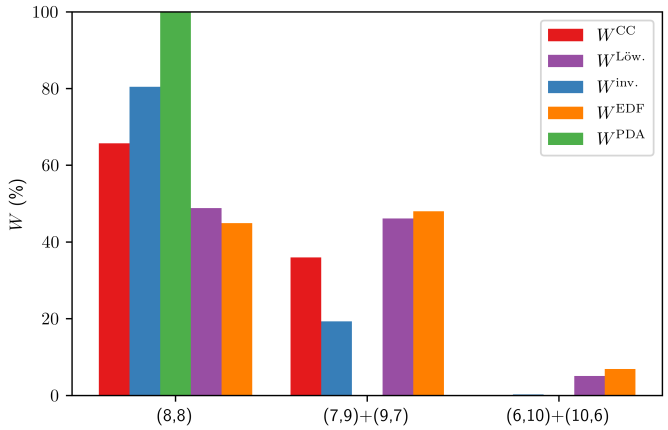

Fig. 12 Weights of groups of VB structures for ethylene. The groups are defined to match with the EDF partitions.

4.3.2 Ozone and Sulfur Dioxide

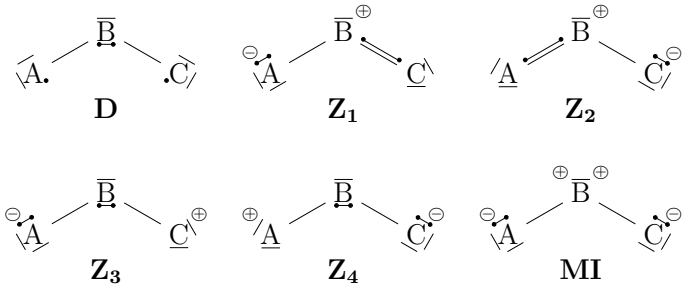

Fig. 13 Six structures of the π system in general 1,3-dipoles. Labels are taken from Braïda et al.[32]

In VB theory, ozone is described best by six π resonance structures, see Figure 13. Harcourt was the first to stress the importance of the diradical 'long bond' structure **D**.[57] Goddard et al.[58] and later Hiberty et al.[59] verified Harcourts assumption with GVB calculations and CASSCF expansions respectively. Wu et al. were the first to perform modern VB calculations on ozone and sulfur dioxide.[60] Braïda et al.[61] explained the reactivity of 1,3-dipoles toward ethylene and acetylene with the weight of the diradical structure, but investigated neither O_3 nor SO_2. Lan et al.[62] then took up that work and investigated ozone and sulfur dioxide with similar modern VB methods. They found ozone to be similar to the dipoles calculated by Braïda et al., but SO_2 dominated by the multi-ionic structure **MI**. Furthermore, they found a good agreement with natural population analysis charges. More recently, Miliordos and Xantheas found ozone to have more diradical character than sulfur dioxide with CASSCF-based icMRCI wave functions although with substantially smaller magnitudes of the diradical contributions.[63] In their work, they adjusted earlier diradicality indices.[64,65] Even more recently, Braïda et al. found a good correlation of some of these indices with VB weights (Chirgwin-Coulson and inverse definition) for 1,3-dipoles built from sulfur and oxygen.[32]

For ozone, the structures **D**, $\mathbf{Z_1}$, and $\mathbf{Z_2}$ are the three most important structures. Thus, the VB wave functions with only these three structures are compared with the full VBSCF wave functions (six structures) and, additionally, with the CAS and HF wave functions. The CAS analogue to the VBSCF wave functions built with the six π structures of Figure 13 is CASSCF(4,3).

The dominant attractors of ozone in PDA with VBSCF(4,3)/BFD-VTZ are shown in Figure 14. Two σ bond electron pairs, the lone pairs, and one additional pair are indicated with a line in the figure. These attractors can clearly be identified with the VB structures **D**, $\mathbf{Z_1}$, and $\mathbf{Z_2}$. Since the σ orbitals are inactive in the VB wave function, both covalent and ionic electron arrangements are found for the two σ bonds, analogously to the attractors in H_2 discussed above. Nonetheless, all ionic and covalent arrangements in the σ bonds can can still be mapped to the VB structures **D**, $\mathbf{Z_1}$, or $\mathbf{Z_2}$, see Figure 17 in the Appendix. Analogous attractors are found for SO_2 with a corresponding three-structure VBSCF(4,3)/BFD-VTZ wave function (Fig. 15). Here, the σ electron pairs are always on the oxygen side, which is expected for polar bonds treated on single-configuration level (i.e. inactive in the VB wave function). The weights of the VB wave functions for O_3 and SO_2 are shown in Figure 16 with the weights for the three-structure VB wave functions displayed on the left sides of the diagrams. For the three-structure wave functions, the PDA weights are in good agreement with all VB weights for both systems and, as described in the literature, the weight of the diradical structure **D** is larger in ozone. The additional three structures ($\mathbf{Z_3}$, $\mathbf{Z_4}$, **MI**) do not change the picture for ozone as the additional weights are small. For sulfur dioxide however, the multi-ionic structure **MI** is roughly as important as the diradical structure **D** according to the three established VB weight definitions. In contrast to these definitions, the PDA weight of the multi-ionic structure **MI** is nearly 100% (only the zwitterionic structures $\mathbf{Z_1}$ and $\mathbf{Z_2}$ have a non-zero PDA weight of $\approx 0.03\%$). The dominating **MI** attractor is shown in Figure 15a. For the CAS wave function of ozone, the weights are in almost perfect agreement with the full VB wave function weights shown in Figure 16a. The HF wave

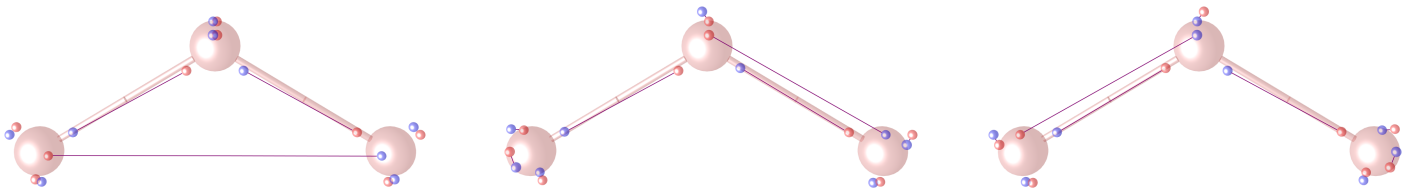

(a) D (88.2 %) **(b) Z_1** (5.7 %) **(c) Z_2** (5.7 %)

Fig. 14 Three attractors of ozone with VBSCF(4,3). PDA weights in brackets. The oxygen nuclei are depicted as red spheres, electrons as small red or blue spheres depending on their m_s quantum number. Pairs of spin-up and spin-down electrons are connected by purple lines in order to highlight the resemblance to the VB structures.

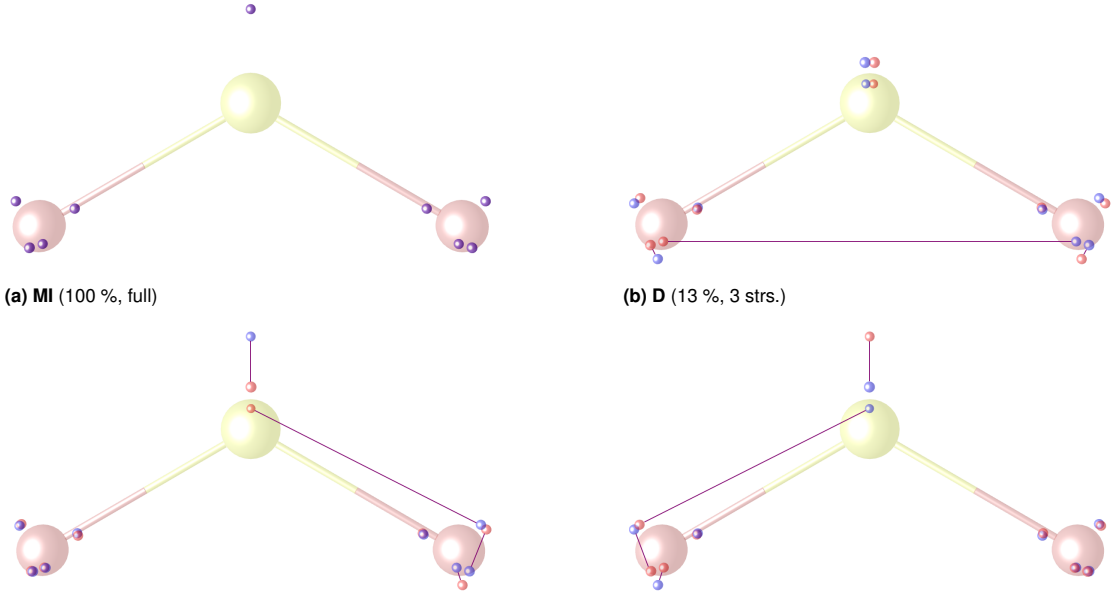

(a) MI (100 %, full) **(b) D** (13 %, 3 strs.)

(c) Z_1 (43 %, 3 strs.) **(d) Z_2** (43 %, 3 strs.)

Fig. 15 Four attractors of sulfur dioxide with VBSCF(4,3). PDA weights in brackets. The oxygen nuclei are depicted as red spheres, the sulfur nucleus as a yellow sphere, electrons as small red or blue spheres depending on their m_s quantum number. Pairs of spin-up and spin-down electrons are connected by purple lines in order to highlight the resemblance to the VB structures.

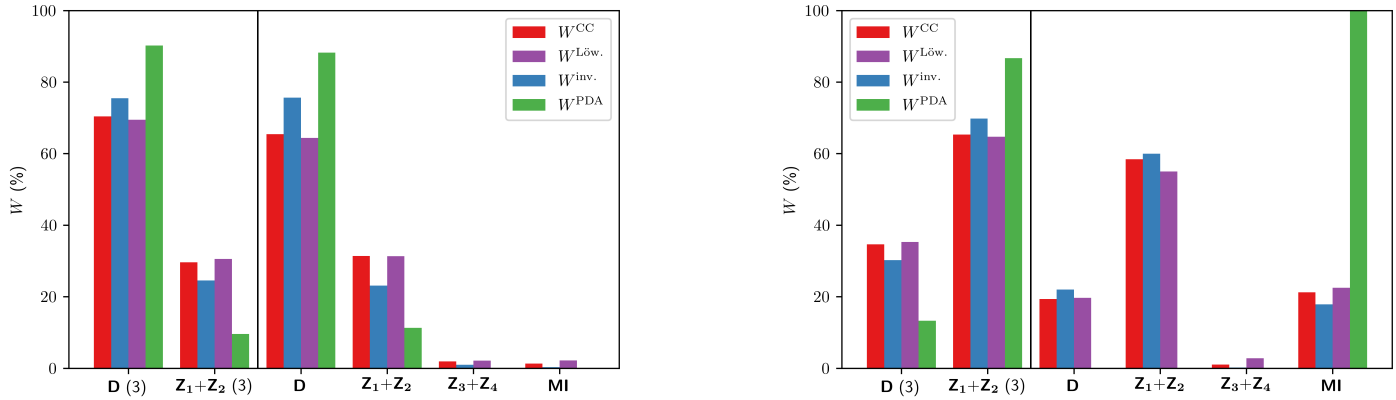

(a) ozone **(b)** sulfur dioxide

Fig. 16 Structure weights for the VB wave functions of ozone and sulfur dioxide. Weights of the three-structure wave functions on the left, respectively.

function of ozone is qualitatively different with the multi-ionic structure **MI** and the zwitterionic structures ($\mathbf{Z_1}$, $\mathbf{Z_2}$) dominating by PDA weight. HF, CAS, and the full VB wave function for sulfur dioxide all result in a multi-ionic (**MI**) PDA weight of 100%. The agreement of HF with CAS is not surprising as the weight of the HF determinant in the CASSCF function is 96% compared to 80% for ozone. Overall, PDA confirms the qualitative difference between ozone and sulfur dioxide described by VB methods with ozone dominated by the diradical electron arrangement while in sulfur dioxide the multi-ionic arrangement is important.

5 Conclusion

In order to compare real space methods with VB theory, a PDA structure weight has been defined and calculated together with the EDF weight by Martín Pendás and coworkers. There are three notable advantages of these two definitions over the established VB weights: first, they are applicable to any wave function. Second, they are still meaningful in the basis set limit where VB theory collapses. And third, they are (theoretically) applicable to experimental probability distributions. Both real space weight definitions give results comparable to VB theory.

The analytical calculations for H_2 showed that the EDF weight is close to the Löwdin one, but qualitatively different from the other definitions. This result was confirmed for the homoatomic single bonds and for the partitions in ethylene. The PDA weight is best compared to the inverse weight of VB theory.

While the PDA results for ozone agree well with the VB weights and the contributions discussed in the literature, the results for SO_2 show a large deviation from the VB weights. Yet, the PDA results can also explain the different reactivities of the two 1,3-dipoles.

Overall, PDA has proven to be a powerful tool that captures the many-electron nature of molecular wave functions and may become an important contribution to modern bond classification.

Conflicts of interest

There are no conflicts to declare.

Acknowledgements

The symbolic mathematics for H_2 have been verified with SymPy.[66] The H_2 integrals s and I have been calculated with NumPy[67] and SciPy.[68] Figures 1 and 13 have been created with the Latex package chemfig.[69] Figure 2 has been created with Plotly.[70] Figures 3, 5, 6, 7, 9, and 16 have been created with Matplotlib.[71] Figures 4, 11, 14, 15, and 17 have been created with the in-house code inPsights by Michael Heuer. Figure 8 has been created with wxMacMolPlt.[72] Figure 10 has been created with the Latex package chemmacros.[73]

Appendix

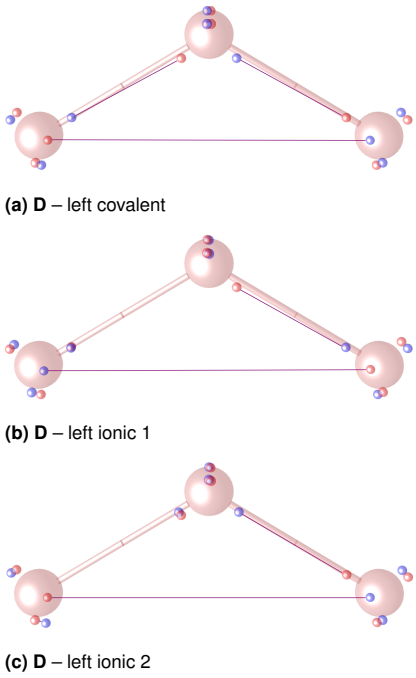

Fig. 17 Three attractors of ozone with VBSCF(4,3). The oxygen nuclei are depicted as red spheres, electrons as small red or blue spheres depending on their m_s quantum number. Pairs of spin-up and spin-down electrons are connected by purple lines in order to highlight the resemblance to the VB structures.

References

1 E. Schrödinger, *Ann. Phys.*, 1926, **384**, 361–376.
2 G. N. Lewis, *J. Am. Chem. Soc.*, 1913, **35**, 1448–1455.
3 G. N. Lewis, *J. Am. Chem. Soc.*, 1916, **38**, 762–785.
4 W. Heitler and F. London, *Z. Phys.*, 1927, **44**, 455–472.
5 L. Pauling, *J. Am. Chem. Soc.*, 1931, **53**, 1367–1400.
6 J. van Lenthe and G. Balint-Kurti, *Chem. Phys. Lett.*, 1980, **76**, 138–142.
7 P. C. Hiberty and S. Shaik, *Theor. Chem. Acc.*, 2002, **108**, 255–272.
8 R. F. W. Bader and P. M. Beddall, *J. Chem. Phys.*, 1972, **56**, 3320–3329.
9 R. F. W. Bader and T. Nguyen-Dang, *Advances in Quantum Chemistry*, Academic Press, Inc., 14th edn, 1981, pp. 63–124.
10 R. F. W. Bader, *Chem. Rev.*, 1991, **91**, 893–928.
11 E. Chamorro, P. Fuentealba and A. Savin, *J. Comput. Chem.*, 2003, **24**, 496–504.
12 E. Francisco, A. Martín Pendás and M. A. Blanco, *J. Chem. Phys.*, 2007, **126**, 094102.
13 E. Francisco, A. Martín Pendás and M. Blanco, *Comput. Phys. Commun.*, 2008, **178**, 621–634.
14 A. Martín Pendás, E. Francisco and M. A. Blanco, *J. Chem. Phys.*, 2007, **127**, 144103.

15 A. Martín Pendás, E. Francisco and M. A. Blanco, *J. Phys. Chem. A*, 2007, **111**, 1084–1090.

16 A. Martín Pendás, E. Francisco and M. A. Blanco, *Phys. Chem. Chem. Phys.*, 2007, **9**, 1087–1092.

17 A. Martín Pendás and E. Francisco, *ChemPhysChem*, 2019, **20**, 2722–2741.

18 L. Zhang, F. Ying, W. Wu, P. C. Hiberty and S. Shaik, *Chem. - Eur. J.*, 2009, **15**, 2979–2989.

19 D. Ferro-Costas and R. A. Mosquera, *Chem. Phys. Lett.*, 2015, **618**, 83–88.

20 A. Martín Pendás and E. Francisco, *Phys. Chem. Chem. Phys.*, 2018, **20**, 12368–12372.

21 A. Scemama, M. Caffarel and A. Savin, *J. Comput. Chem.*, 2007, **28**, 442–454.

22 K. Artmann, *Z. Naturforsch. A*, 1946, **1**, 426–432.

23 H. K. Zimmerman and P. Van Rysselberghe, *J. Chem. Phys.*, 1949, **17**, 598–602.

24 A. Lüchow and R. Petz, *J. Comput. Chem.*, 2011, **32**, 2619–2626.

25 A. Lüchow, *J. Comput. Chem.*, 2014, **35**, 854–864.

26 C. Schulte and A. Lüchow, *Recent Progress in Quantum Monte Carlo*, American Chemical Society, 2016, pp. 89–105.

27 Y. Liu, T. J. Frankcombe and T. W. Schmidt, *Phys. Chem. Chem. Phys.*, 2016, **18**, 13385–13394.

28 Y. Liu, P. Kilby, T. J. Frankcombe and T. W. Schmidt, *Nat. Commun.*, 2018, **9**, 1436.

29 Y. Liu, P. Kilby, T. J. Frankcombe and T. W. Schmidt, *Chem. Sci.*, 2019, **10**, 6809–6814.

30 Y. Liu, P. Kilby, T. J. Frankcombe and T. W. Schmidt, *Nat. Commun.*, 2020, **11**, 1210.

31 M. Waitz, R. Y. Bello, D. Metz, J. Lower, F. Trinter, C. Schober, M. Keiling, U. Lenz, M. Pitzer, K. Mertens, M. Martins, J. Viefhaus, S. Klumpp, T. Weber, L. P. H. Schmidt, J. B. Williams, M. S. Schöffler, V. V. Serov, A. S. Kheifets, L. Argenti, A. Palacios, F. Martín, T. Jahnke and R. Dörner, *Nat. Commun.*, 2017, **8**, 2266.

32 B. Braïda, S. E. Galembeck and P. C. Hiberty, *J. Chem. Theory Comput.*, 2017, **13**, 3228–3235.

33 P. Löwdin, *J. Chem. Phys.*, 1950, **18**, 365–375.

34 G. A. Gallup and J. M. Norbeck, *Chem. Phys. Lett.*, 1973, **21**, 495–500.

35 L. Song, Y. Mo, Q. Zhang and W. Wu, *J. Comput. Chem.*, 2005, **26**, 514–521.

36 Z. Chen, F. Ying, X. Chen, J. Song, P. Su, L. Song, Y. Mo, Q. Zhang and W. Wu, *Int. J. Quantum Chem.*, 2015, **115**, 731–737.

37 M. J. Frisch, G. W. Trucks, H. B. Schlegel, G. E. Scuseria, M. A. Robb, J. R. Cheeseman, G. Scalmani, V. Barone, G. A. Petersson, H. Nakatsuji, X. Li, M. Caricato, A. V. Marenich, J. Bloino, B. G. Janesko, R. Gomperts, B. Mennucci, H. P. Hratchian, J. V. Ortiz, A. F. Izmaylov, J. L. Sonnenberg, D. Williams-Young, F. Ding, F. Lipparini, F. Egidi, J. Goings, B. Peng, A. Petrone, T. Henderson, D. Ranasinghe, V. G. Zakrzewski, J. Gao, N. Rega, G. Zheng, W. Liang, M. Hada, M. Ehara, K. Toyota, R. Fukuda, J. Hasegawa, M. Ishida, T. Nakajima, Y. Honda, O. Kitao, H. Nakai, T. Vreven, K. Throssell, J. A. Montgomery Jr., J. E. Peralta, F. Ogliaro, M. J. Bearpark, J. J. Heyd, E. N. Brothers, K. N. Kudin, V. N. Staroverov, T. A. Keith, R. Kobayashi, J. Normand, K. Raghavachari, A. P. Rendell, J. C. Burant, S. S. Iyengar, J. Tomasi, M. Cossi, J. M. Millam, M. Klene, C. Adamo, R. Cammi, J. W. Ochterski, R. L. Martin, K. Morokuma, O. Farkas, J. B. Foresman and D. J. Fox, *Gaussian 16 Revision C.01*, 2016.

38 H.-J. Werner, P. J. Knowles, G. Knizia, F. R. Manby, M. Schütz, P. Celani, W. Györffy, D. Kats, T. Korona, R. Lindh, A. Mitrushenkov, G. Rauhut, K. R. Shamasundar, T. B. Adler, R. D. Amos, S. J. Bennie, A. Bernhardsson, A. Berning, D. L. Cooper, M. J. O. Deegan, A. J. Dobbyn, F. Eckert, E. Goll, C. Hampel, A. Hesselmann, G. Hetzer, T. Hrenar, G. Jansen, C. Köppl, S. J. R. Lee, Y. Liu, A. W. Lloyd, Q. Ma, R. A. Mata, A. J. May, S. J. McNicholas, W. Meyer, T. F. Miller III, M. E. Mura, A. Nicklass, D. P. O'Neill, P. Palmieri, D. Peng, K. Pflüger, R. Pitzer, M. Reiher, T. Shiozaki, H. Stoll, A. J. Stone, R. Tarroni, T. Thorsteinsson, M. Wang and M. Welborn, *MOLPRO, version 2019.2, a package of ab initio programs*, 2019.

39 *NIST Computational Chemistry Comparison and Benchmark Database NIST Standard Reference Database Number 101 Release 20, August 2019, Editor: Russell D. Johnson III (http://cccbdb.nist.gov/)*.

40 *NIST Diatomic Spectral Database (www.physics.nist.gov)*.

41 R. L. Redington, W. B. Olson and P. C. Cross, *J. Chem. Phys.*, 1962, **36**, 1311–1326.

42 G. Herzberg, *Molecular Spectra & Molecular Structure III. Electronic Spectra and Electronic Structure of Polyatomic Molecules*, D. Van Nostrand Company, Inc., Princeton, NJ, 1966.

43 M. Tsuboi and J. Overend, *J. Mol. Spectrosc.*, 1974, **52**, 256–268.

44 K. P. Huber and G. Herzberg, *Molecular Spectra and Molecular Structure*, Springer US, Boston, MA, 1979.

45 A. Hoy and P. Bunker, *J. Mol. Spectrosc.*, 1979, **74**, 1–8.

46 *Structure of Free Polyatomic Molecules*, ed. K. Kuchitsu, Springer Berlin Heidelberg, Berlin, Heidelberg, 1998.

47 E. van Lenthe and E. J. Baerends, *J. Comput. Chem.*, 2003, **24**, 1142–1156.

48 K. O-ohata, H. Taketa and S. Huzinaga, *J. Phys. Soc. Jpn.*, 1966, **21**, 2306–2313.

49 G. A. Petersson, S. Zhong, J. A. Montgomery and M. J. Frisch, *J. Chem. Phys.*, 2003, **118**, 1101–1109.

50 M. Burkatzki, C. Filippi and M. Dolg, *J. Chem. Phys.*, 2007, **126**, 234105.

51 A. D. Becke, *J. Chem. Phys.*, 1988, **88**, 1053–1062.

52 C. Lee, W. Yang and R. G. Parr, *Phys. Rev. B*, 1988, **37**, 785–789.

53 A. D. Becke, *J. Chem. Phys.*, 1993, **98**, 5648–5652.

54 P. J. Stephens, F. J. Devlin, C. F. Chabalowski and M. J. Frisch, *J. Phys. Chem.*, 1994, **98**, 11623–11627.

55 S. H. Vosko, L. Wilk and M. Nusair, *Can. J. Phys.*, 1980, **58**,

1200–1211.

56 T. Helgaker, P. Jørgensen and J. Olsen, *Molecular Electronic-Structure Theory*, John Wiley & Sons, Ltd, Chichester, UK, 2000.

57 R. Harcourt, *J. Mol. Struct.*, 1972, **12**, 351–366.

58 W. A. Goddard, T. H. Dunning, W. J. Hunt and P. J. Hay, *Acc. Chem. Res.*, 1973, **6**, 368–376.

59 P. C. Hiberty and C. Leforestier, *J. Am. Chem. Soc.*, 1978, **100**, 2012–2017.

60 W. Wu, Y.-R. Mo and Q.-E. Zhang, *Chin. J. Chem.*, 1993, **11**, 490–498.

61 B. Braïda, C. Walter, B. Engels and P. C. Hiberty, *J. Am. Chem. Soc.*, 2010, **132**, 7631–7637.

62 Y. Lan, S. E. Wheeler and K. N. Houk, *J. Chem. Theory Comput.*, 2011, **7**, 2104–2111.

63 E. Miliordos and S. S. Xantheas, *J. Am. Chem. Soc.*, 2014, **136**, 2808–2817.

64 W. D. Laidig and H. F. Schaefer, *J. Chem. Phys.*, 1981, **74**, 3411–3414.

65 V.-A. Glezakou, S. T. Elbert, S. S. Xantheas and K. Ruedenberg, *J. Phys. Chem. A*, 2010, **114**, 8923–8931.

66 A. Meurer, C. P. Smith, M. Paprocki, O. Čertík, S. B. Kirpichev, M. Rocklin, A. Kumar, S. Ivanov, J. K. Moore, S. Singh, T. Rathnayake, S. Vig, B. E. Granger, R. P. Muller, F. Bonazzi, H. Gupta, S. Vats, F. Johansson, F. Pedregosa, M. J. Curry, A. R. Terrel, Š. Roučka, A. Saboo, I. Fernando, S. Kulal, R. Cimrman and A. Scopatz, *PeerJ Comput. Sci.*, 2017, **3**, e103.

67 S. van der Walt, S. C. Colbert and G. Varoquaux, *Comput. Sci. Eng.*, 2011, **13**, 22–30.

68 P. Virtanen, R. Gommers, T. E. Oliphant, M. Haberland, T. Reddy, D. Cournapeau, E. Burovski, P. Peterson, W. Weckesser, J. Bright, S. J. van der Walt, M. Brett, J. Wilson, K. Jarrod Millman, N. Mayorov, A. R. Nelson, E. Jones, R. Kern, E. Larson, C. J. Carey, I. Polat, Y. Feng, E. W. Moore, J. Vand erPlas, D. Laxalde, J. Perktold, R. Cimrman, I. Henriksen, E. Quintero, C. R. Harris, A. M. Archibald, A. H. Ribeiro, F. Pedregosa, P. van Mulbregt and S. . . Contributors, *Nat. Methods*, 2020, **17**, 261–272.

69 C. Tellechea, *chemfig v1.5 Draw molecule with an easy syntax*, 2020, `https://www.ctan.org/pkg/chemfig`.

70 P. T. Inc., *Collaborative data science*, 2015, `https://plot.ly`.

71 J. D. Hunter, *Comput. Sci. Eng.*, 2007, **9**, 90–95.

72 B. M. Bode and M. S. Gordon, *J. Mol. Graphics Modell.*, 1998, **16**, 133–138.

73 C. Niederberger, *chemmacros v5.10 comprehensive support for typesetting chemistry documents*, 2020, `https://www.ctan.org/pkg/chemmacros`.